35. Sullenger, B.A.; Gallardo, H.F.; Ungers, G.E.; Gilboa, E. Over expression of TAR sequences renders cells resistant to human immunodeficiency virus replication. Cell **1990**, 63, 601–603.
36. Sarver, N.; Cantin, E.M.; Chang, P.S.; Zaia, J.A.; Ladne, P.A.; Stephens, D.A.; Rossi, J.J. Ribozymes as potential anti-HIV-1 therapeutic agents. Science **1990**, 247, 1222–1225.
37. Yu, M.; Poeschla, E.; Wong-Staal, F. Progress towards gene therapy for HIV infection. Gene Ther. **1994**, 1, 13–26.
38. Liu, J.; Woffendin, C.; Yang, Z.Y.; Nabel, G.J. Regulated expression of a dominant negative form of Rev improves resistance to HIV replication in T cells. Gene Ther. **1994**, 1, 32–37.
39. Malim, M.H.; Bohnlein. S.; Hauber, J.; Cullen, B.R. Functional dissection of the HIV-1 Rev trans-activator-derivation of a trans-dominant repressor of Rev function. Cell **1989**, 58, 205–214.
40. Sczakiel, G.; Homann, M.; Rittner, K. Computer-aided search for effective antisense RNA target sequences of the human immunodeficiency virus type 1. Antisense Res. Dev. **1993**, 3, 45–52.
41. Biasolo, M.A.; Radaelli, A.; del Pup, L.; Franchin, E.; De Giuli-Morghen, C.; Palu, G. A new antisense tRNA construct for the genetic treatment of human immunodeficiency virus type 1 infection. J. Virol. **1996**, 70, 2154–2161.
42. Cohli, H.; Fan, B.; Joshi, R.L.; Ramezani, A.; Li, X.; Joshi, S. Inhibition of HIV-1 multiplication in a human CD4+ lymphocytic cell line expressing antisense and sense RNA molecules containing HIV-1 packaging signal and Rev response element(s). Antisense Res. Dev. **1994**, 4, 19–29.
43. Joshi, S.; Van Brunschot, A.; Asad, S.; van der Elst, I.; Read, S.E.; Bernstein, A. Inhibition of human immunodeficiency virus type 1 multiplication by antisense and sense RNA expression. J. Virol. **1991**, 65, 5524–5530.
44. Bitko, V.; Barik, S. Phenotypic silencing of cytoplasmic genes using sequence-specific double-stranded short interfering RNA and its application in the reverse genetics of wild type negative-strand RNA viruses. BMC Microbiol. **2001**, 1, 34–45.
45. Sharp, P.A. RNA interference. Genes Dev. **2001**, 15, 485–490.
46. Shahabuddin, M.; Khan, A.S. Inhibition of human immunodeficiency virus type 1 by packageable, multigenic antisense RNA. Antisense Nucleic Acid. Drug Dev. **2000**, 10, 141–145.
47. Torrence, P.F.; Maitra, R.K.; Lesiak, K.; Khamnei, S.; Zhou, A.; Silverman, R.H. Targeting RNA for degradation with a (2′-5′) oligoadenylate-antisense chimera. Proc. Natl. Acad. Sci. USA **1993**, 90, 1300–1304.
48. Sakai, A.; Hirabashi, Y.; Aizawa, S.; Tanaka, M.; Ida, S.; Oka, S. Investigation of a new p24 antigen detection system by the chemiluminescence-enzyme-immuno-assay. J. Japn. Assoc. Infect. Dis. **1999**, 73, 205–212.
49. Akari, H.; Fukumori, T.; Adachi, A. Cell-dependent requirement of Human Immunodeficiency Virus Type 1 gp41 cytoplasmic tail for env incorporation in virions. J. Virol. **2000**, 74, 4891–4893.
50. Broder, Y.C.; Stanhill, A.; Zakai, N.; Friedler, A.; Gilon, C.; Loyter, A. Translocation of NLS-BSA conjugates into nuclei of permeabilized mammalian cells can be supported by protoplast extract: An experimental system for studying plant cytosol factors involved in nuclear import. FEBS Lett. **1997**, 412, 535–539.
51. Miura, Y.; Misawa, N.; Meada, N.; Inagaki, Y.; Tanaka, Y.; Ito, M.; Koyagaki, N.; Yamamoto, N.; Yagita, H.; Mizusawa, H.; Koyanagi, Y. Contribution of tumor necrosis factor-related apoptosis-inducing ligand (TRAIL) to apoptosis of human CD4+T cells in HIV-1 infected hu-PBL-NOD-SCID mice. J. Exp. Med. **2001**, 193, 651–659.
52. Adachi, A.; Gendelman, H.E.; Koenig, S.; Folks, T.; Willey, R.; Rabson, A.; Martin, M.A. Production of acquired immunodeficiency syndrome-associated retrovirus in human and nonhuman cells transfected with an infectious molecular clone. J. Virol. **1986**, 59, 284–291.
53. Reed, L.J.; Muench, H.A. A simple method of estimating fifty percent endpoints. Am. J. Hyg. **1938**, 27, 493–497.

Nucleosides, Nucleotides, and Nucleic Acids, 24 (5–7):431–434, (2005)

ISSN: 1525-7770 print/ 1532-2335 online
DOI: 10.1081/NCN-200059981

Taylor & Francis
Taylor & Francis Group

LENTIVIRAL-MEDIATED DELIVERY OF COMBINED HIV-1 DECOY TAR AND Vif siRNA AS A SINGLE RNA MOLECULE THAT CLEAVES TO INHIBIT HIV-1 IN TRANSDUCED CELLS

Jacob Samson Barnor ▫ *Department of Life and Environmental Science, Chiba Institute of Technology, Chiba, Japan and Noguchi Memorial Institute for Medical Research, Department of Virology, Legon-Accra, Ghana*

Naoko Miyano-Kurosaki ▫ *Department of Life and Environmental Science, Chiba Institute of Technology and High Technology Research Center, Chiba, Japan*

Kazuya Yamaguchi and Yusuke Abumi ▫ *Department of Life and Environmental Science, Chiba Institute of Technology, Chiba, Japan*

Koichi Ishikawa and Naoki Yamamoto ▫ *National Institute of Infectious Diseases, AIDS Research Center, Shinjuku-ku, Tokyo*

Hiroshi Takaku ▫ *Department of Life and Environmental Science, Chiba Institute of Technology, Chiba, Japan and High Technology Research Center, Chiba, Japan*

▫ *RNA interference (RNA_i) silences gene expression via short interfering 21–23 mer double-stranded RNA (siRNA) segments that guide cognate mRNA degradation in a sequence-specific manner. On the other hand, HIV-1 decoy TAR RNA are known to competitively interact with the HIV-1 Tat protein, to downregulate the enhanced gene expression from the long terminal repeat (LTR) promoters. Here we report that a novel expression construct, encoding both HIV-1 decoy TAR and Vif siRNA, as a single RNA substrate, was expressed under the control of the human U6 promoter, and later the TAR and siRNA were cleaved into their respective separate RNA by the endogenous RNase III-like enzyme. Each of the cleaved HIV-1 anti-genes then synergistically contributed toward enhancing the inhibition efficacy (>80%) of HIV-1 replication in transduced Jurkat cells. These results suggest that targeting HIV-1 mRNA with simultaneously expressed intracellular decoy TAR and Vif-siRNA could lead to an effective gene therapy strategy for the control and management of HIV-AIDS.*

This work was supported in part by a Grant-in-Aid for High Technology Research from the Ministry of Education, Science, Sports and Culture, Japan, a grant from the Sasakawa Foundation, and a Research Grant from the Human Science Foundation (HIV-SA-14719).

Address correspondence to Jacob Samson Barnor, Noguchi Memorial Institute for Medical Research, Department of Virology, P.O. Box LG, Legon-Accra 581, Ghana.

INTRODUCTION

The role of double-stranded RNA (dsRNA) as a potent silencer of homologous genes in the nematode *Caenorhabditis elegans* was unveiled through the pioneering work of Fire et al.[1] in 1998. This technique, termed as RNA interference (RNAi), has proven to be a powerful tool and has been used to disrupt the function of genes in both plants and animals. Recently, the use of RNAi has been extended to differentiated cultured mammalian cells.[2] Importantly, siRNA expressed from DNA templates are able to silence gene expression as effective as exogenously introduced synthetic siRNA. RNAi and other gene therapy strategies have been effectively used to inhibit the replication of several different pathogenic viruses including HIV-1, by targeting the Gag-Pol, Env, Vif, and the small regulatory proteins, such as Tat and Rev, in culture.[3] In this study, we have combined the RNAi and HIV-1 decoy TAR RNA mechanisms via a single RNA molecule, delivered for intracellular expression by a novel lentiviral-based vector construct (CS-Vif siRNA-TAR) under the control of the human U6 promoter, which was later cleaved in the cells by the endogenous RNase III-like enzyme. The dual HIV-1 anti-genes efficiently inhibited HIV-1 replication in a dose-dependent manner. They further mediated a substantial down-regulation of the HIV-1 viral Vif mRNA and the reporter gene (EGFP) expression in transduced Jurkat cells. Our results have provide clear evidence that targeting the HIV-1 genes with simultaneously expressed intracellular dual HIV-1 anti-genes, such as Vif siRNA and decoy TAR RNA, could be a promising gene therapy approach for HIV-1.

RESULTS AND DISCUSSION

To evaluate the enhancement of siRNA in the sequence-specific inhibition of HIV-1 replication, we constructed the U6 vectors (Figure 1A) by linking the HIV-1 Vif siRNA with the decoy TAR, and assessed the mRNA expression in HeLa $CD4^+$

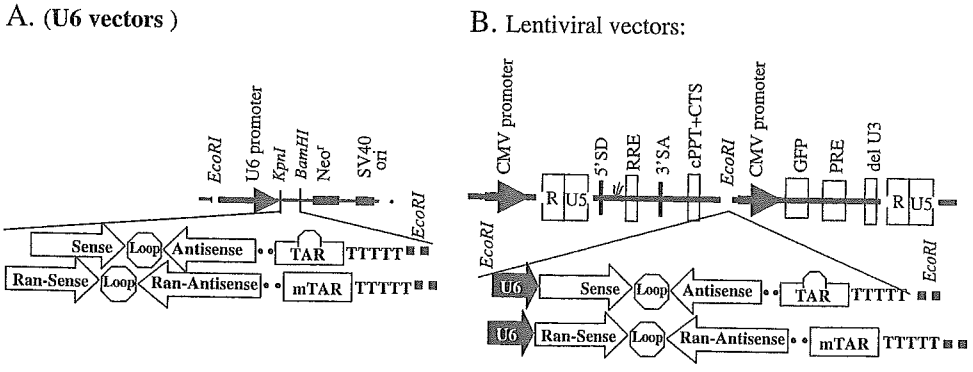

FIGURE 1 Construction of the U6 plasmid and lentiviral vectors. A. Sense and antisense strands of the synthetic DNA oligonucleotides were annealed at 95°C for 5 min, and cloned into the KpnI and BamHI cloning sites in the U6 vector. B. The EcoRI sites upstream from the U6 promoter and downstream from the terminating sequence of the generated U6 vectors were digested, and the fragments were cloned into the CS-CDF-CG-PRE vector to generate the lentiviral vectors.

cells (3×10^5) transfected with the Lipofectamine 2000 reagent. Northern blot analysis of total RNA extracted with Trizol showed an in vivo cleavage activity of the RNA molecule 72 h post-transfection in the cells. Further in-vitro cleavage assays using recombinant human dicer proved that the Vif siRNA-decoy TAR RNA substrate was mostly cleaved into its separate components, as the Vif siRNA and decoy TAR RNA, respectively (data not shown).

We then examined the dose-dependent anti-HIV-1 efficacy of the RNA substrate by co-transfecting various amounts (0.1, 1.0, and 3.0 μg) of U6 vector DNA and 0.2 μg of HIV-1 plasmid DNA into HeLa $CD4^+$ cells, and measuring the HIV-1 gag p24 antigen production level from the cell-free culture supernatant by a chemiluminescence enzyme-linked immunosorbent assay system (CLEIA) after 72 h, as an index for inhibition. The highest inhibition was observed at a concentration of 3 μg U6 vector DNA, while at the 1 μg U6 vector DNA concentration, there was still an appreciable level of inhibition. The decoy TAR U6 vector alone at 3 μg DNA did not mediate as much inhibition as that of the Vif siRNA U6 vector alone at 3 μg DNA. Our results therefore suggest that the TAR component of the U6 Vif siRNA-decoy TAR RNA molecule only complemented the inhibition efficacy in the co-transfected cells. The observed inhibitions correlated with the down-regulation of the HIV-1 viral mRNA (data not shown).

We further elucidated the inhibitory capacity of the RNA substrate, by constructing the lentiviral versions of the U6 plasmid Vif siRNA-TAR and Vif Ran-mTAR vectors (Figure 1B). 293T cells were transfected by the calcium phosphate precipitation method, and the viral titers of transduced MT-4 cells (3×10^5) were calculated using the expressed EGFP from FACS analysis. Jurkat cells (5×10^5) were then transduced with 10 MOI of the lentivirus expressing the Vif siRNA-TAR, including its random siRNA-mutant TAR version in addition to mock transduced Jurkat cells as control,[4] and were finally challenged with 0.02 MOI of $HIV\text{-}1_{NL4\text{-}3}$.

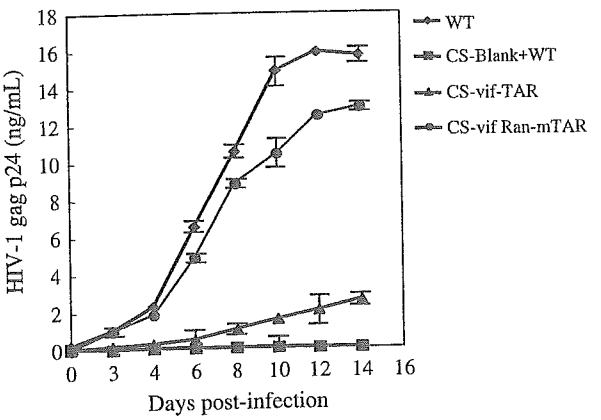

FIGURE 2 Evaluation of the inhibition efficacy of the trans-genes. Transiently transduced Jurkat cells expressing the Vif-TAR, Ran-Vif-mTAR and empty lenti-vectors were challenged with 0.02 MOI of $HIV\text{-}1_{NLE}$ and cultured over a period of 14 days. Cell-free supernatants were sampled over the period and analyzed for HIV-1 *gag p24* antigen production by CLEIA. Data represent the mean values in the supernatants ± SD of three independent experiments.

Cell-free culture supernatants were sampled over a period of 14 days and evaluated for HIV-1 gag p24 antigen production, to determine the sustainable inhibition efficacy of the lentivirus-delivered dual HIV-1 anti-genes. The results indicated the sustained inhibition of HIV-1 replication by the lentivirus-mediated Vif siRNA-TAR RNA molecule, compared to the lentivirus-mediated random siRNA-mutated TAR version (Vif Ran siRNA-mTAR), the positive controls (lentivirus-mediated CS-empty vector + HIV-1_{NL4-3}. (wt)), and the mock infected, empty vector transduced Jurkat cells (negative control) over the same period of 14 d (Figure 2). In conclusion, our findings suggest that targeting the HIV-1 genes with the intracellularly expressed HIV-1Vif siRNA and decoy TAR RNA, as a single RNA substrate, enhances both delivery efficiency to the target cells and the inhibition efficacy on HIV-1 replication. This strategy will be a promising tool for HIV-1 gene therapy.

REFERENCES

1. Fire, A.; Xu, S.-Q.; Montgomery, M.K.; Kostas, S.A.; Driver, S.E.; Mello, C.C. Potent and specific genetic interference by double-stranded RNA in caenorhabditis elegans. Nature **1998**, *391*, 806–811.
2. Elbashir, S.M.; Harborth, J.; Lendeckel, W.; Yalcin, A.; Welber, K.; Tuschl, T. Duplexes of 21-nucleotide RNAs mediate RNA interference in mammaliam cell culture. Nature **2001**, *411*, 494–498.
3. Barnor, J.S.; Miyano-Kurosaki, N.; Yamaguchi, K.; Sakamoto, A.; Ishikawa, K.; Inagaki, Y.; Yamamoto, N.; Osei-Kwasi, M.; Ofori-Adjei, D.; Takaku, H. Intracellular expression of antisense RNA transcripts complementary to the human immunodeficiency virus type-1 Vif gene inhibits viral replication in infected T-lymphoblastoid cells. Biochem. Biophys. Res. Commun. **2004**, 544–550.
4. Brummelkamp, T.R.; Bernards, R.; Agami, R.A. System for stable expression of short interfering RNAs in mammalian cells. Science **2002**, *296*, 550–553.

Published online January 12, 2005

Nucleic Acids Research, 2005, Vol. 33, No. 1 **235–243**
doi:10.1093/nar/gki164

Inhibition of HIV-1 gene expression by retroviral vector-mediated small-guide RNAs that direct specific RNA cleavage by tRNase ZL

Yuichiro Habu[2], Naoko Miyano-Kurosaki[1,2], Michiko Kitano[1], Yumihiko Endo[1], Masakazu Yukita[1], Shigeru Ohira[1], Hiroaki Takaku[3], Masayuki Nashimoto[3] and Hiroshi Takaku[1,2,*]

[1]Department of Life and Environmental Sciences and [2]High Technology Research Center, Chiba Institute of Technology, 2-17-1 Tsudanuma, Narashino, Chiba 275-0016, Japan and [3]Department of Applied Life Sciences, Niigata University of Pharmacy and Applied Life Sciences, 265-1 Higashito, Niitsu, Niigata 956-8603, Japan

Received December 6, 2004; Revised and Accepted December 15, 2004

ABSTRACT

The tRNA 3′-processing endoribonuclease (tRNase Z or 3′ tRNase; EC 3.1.26.11) is an essential enzyme that removes the 3′ trailer from pre-tRNA. The long form (tRNase ZL) can cleave a target RNA *in vitro* at the site directed by an appropriate small-guide RNA (sgRNA). Here, we investigated whether this sgRNA/tRNase ZL strategy could be applied to gene therapy for AIDS. We tested the ability of four sgRNA-expression plasmids to inhibit HIV-1 gene expression in COS cells, using a transient-expression assay. The three sgRNAs guide inhibition of HIV-1 gene expression in cultured COS cells. Analysis of the HIV-1 mRNA levels suggested that sgRNA directed the tRNase ZL to mediate the degradation of target RNA. The observation that sgRNA was localized primarily in nuclei suggests that tRNase ZL cleaves the HIV-1 mRNA when complexed with sgRNA in this location. We also examined the ability of two retroviral vectors expressing sgRNA to suppress HIV-1 expression in HIV-1-infected Jurkat T cells. sgRNA-SL4 suppressed HIV-1 expression almost completely in infected cells for up to 18 days. These results suggest that the sgRNA/tRNase ZL approach is effective in downregulating HIV-1 gene expression.

INTRODUCTION

RNA-based gene-interference strategies for the treatment of HIV-1 infection have often used technology based on antisense oligonucleotides, ribozymes or double-stranded interference RNA (RNAi) (1–11). A more recent approach uses external guide sequences (EGSs) to induce cleavage of a target mRNA by endogenous RNase P. This strategy is unique in that cleavage of a specific target mRNA occurs after hybridization of the EGS to form a structure resembling a tRNA substrate (12,13). RNA-based EGSs have been expressed endogenously as transgenes in both bacteria and mammalian cells (12,14) and have been effective in inhibiting gene expression by HIV-1 (15,16). We previously designed a short RNase P-associated EGS to target HIV-1-U5 and evaluated its ability to inhibit HIV-1 replication (17). Mammalian cells contain the essential enzyme, tRNA 3′-processing endoribonuclease (tRNase Z or 3′-tRNase; EC 3.1.26.11), which removes 3′ trailers from pre-tRNAs (18). The human genome contains two tRNase Z genes, which encode a 362 amino acid short form (tRNase ZS) and an 829 amino acid long form (tRNase ZL) (19,20). Although the C-terminal half of tRNase ZL has a high level of similarity to the whole of tRNase ZS, they each require different reaction conditions for optimal activity (20). Interestingly, the human tRNase ZL gene was first identified as a candidate prostate cancer-susceptibility gene (21). Two types of mutation in the human tRNase ZL gene, an insertion/frameshift and a missense change, segregate with prostate cancer in two different pedigrees. Furthermore, two additional common missense mutations seem to be associated with prostate cancer. However, a causal association between the missense mutations and prostate cancer has not been proven, because these amino acid substitutions do not alter the enzymatic activities of tRNase ZL (22). The long-form enzyme is unique in that it can cleave any RNA at any site when directed by a small-guide RNA (sgRNA) *in vitro*

*To whom correspondence should be addressed. Tel: +81 47 478 0407; Fax: +81 47 471 8764; Email: takaku@ic.it-chiba.ac.jp

The authors wish it to be known that, in their opinion, the first two authors should be regarded as joint First Authors

(23–27). tRNase ZL functions in the same way as the 4 nt-recognizing RNA cutter RNase 65, by forming a complex with a 3′-truncated tRNA (23). Partial HIV-1 RNA targets can be cleaved site specifically by the enzyme, once the targets form pre-tRNA-like structures with the aid of appropriate 5′-half-tRNAs (24). RNA heptamers that form acceptor-stem-like duplexes with their targets through base pairing can also direct the specific cleavage of target RNAs by tRNase ZL *in vitro* with the same efficiency as the original 5′-half-tRNAs (25,26). However, in this case, the target sites are restricted to regions immediately downstream of stable hairpin structures resembling the T stem/loop. Together with such flexibility in substrate recognition, the ubiquity and constitutive expression of tRNase ZL suggests that this enzyme can be utilized for specific cleavage of cellular RNAs by introducing the appropriate sgRNAs into living cells (27).

Recently, we demonstrated the efficacy of this method in specifically targeting RNA in living cells by introducing sgRNAs encoded either by expression plasmids or by 2′-*O*-methyl RNAs (28). The expression of the exogenous reporter genes for *Escherichia coli* chloramphenicol acetyltransferase and firefly luciferase were downregulated for at least 48 h by appropriately designed sgRNAs in cultured human and dog cells. A 2′-*O*-methyl heptamer designed to target the endogenous Bcl-2 mRNA was also successful in Sarcoma 180 cells.

In the present study, we investigated whether the sgRNA/tRNase ZL strategy could also be an effective approach to gene therapy for AIDS. Several sgRNAs targeted against HIV-1 mRNA, and expressed by plasmid and retroviral vectors, were tested for their ability to repress its expression. Our findings confirmed that they were effective in both COS and Jurkat cells.

MATERIALS AND METHODS

Plasmid construction and retroviral vector production

Expression cassettes for the sgRNA were constructed under the control of the human methionine tRNA promoter. The expressed sgRNA was targeted against either the packaging signal or the *gag* portion of the HIV-1_{NL4-3} strain (Figure 1B). Enhanced green fluorescent protein (EGFP) is a red-shifted variant of wild-type GFP (29,30), which has been optimized for brighter fluorescence and higher expression in mammalian cells (excitation maximum = 488 nm; emission maximum = 507 nm). A DNA fragment containing EGFP was excised from the plasmid pLEGFP (Promega, Madison, WI) by digestion with BamHI–NaeI. The EGFP fragment was ligated to the EcoRI and XhoI sites of pSV2neo/sgR to generate pSV2neo/sgRG. The Moloney strain of the murine leukaemia virus (MoMLV)-based sgRNA pLsgRGSN (Figure 1B) was constructed by inserting the EcoRI and XhoI fragments from plasmid pSV2neo/sgRG, along with sgRNAs and EGFP genes, into the EcoRI and XhoI sites of the retroviral vector pLXSN (31).

Vesicular stomatitis virus glycoprotein-pseudotyped retrovirus vector supernatants were generated by transient transfection of 293T cells, as described previously (32), using 20 μg of vector plasmid, 10 μg of pMLVΔψΔenv (33) and 10 μg of pVSVG envelope plasmid (32,34). Thereafter, supernatants were collected every 12 h for 3 days, filtered through a 0.45 μm pore-size filter (Nalgene, Rochester, NY) and concentrated 100- to 1000-fold by ultracentrifugation (35,36). Pellets were resuspended in serum-free DMEM and stored at −80°C until they were used.

Transduction of target cells

A total of 3×10^5 Jurkat cells per well were plated out in 6-well plates 1 day before transduction. After 24 h, virus supernatant was added together with polybrene (final concentration = 5–8 μg/ml) and the cells were incubated at 25°C overnight. The medium was then replaced with fresh medium containing G418 (500 μg/ml; GIBCO-BRL, Rockville, MD). After 10 days, cell pools that were resistant to G418 were established.

Cells and transfection

COS and Jurkat cells were grown in RPMI 1640 medium (Sigma, St. Louis, MO) supplemented with 10% (v/v) heat-inactivated fetal bovine serum (FBS) at 37°C in a 5% CO_2 atmosphere. Transfection was carried out using the FuGENE™6 reagent (Roche Diagnostics, Tokyo, Japan) according to the manufacturer's protocol.

Luciferase assay

Luciferase activity was measured with the PicaGene kit (Toyo-inki, Tokyo, Japan) according to the manufacturer's protocol. The envelope-defective HIV-1 NL_{4-3}-based retroviral vector containing a luciferase-expression marker (pNL_{4-3}-luc) (32) was generated as follows. The *nef* gene sequences of the HIV-1 NL_{4-3} genome were substituted with the firefly luciferase gene, and the envelope gene sequences located between two Bgl II restriction endonuclease sites were deleted (Figure 1B). The transfection reagent, FuGENE™6, was used to transfect COS cells with the plasmids expressing sgRNA and pNL_{4-3}-luc. The COS cells were lysed using 200 μl of PicaGene cell lysis buffers (Toyo-inki) for 15 min and detached from the plate by scraping. Cellular debris were then removed by centrifugation. The luminescent signal was quantitated by adding 10 μl clarified lysate to 100 μl luminous substrate, and the level of fluorescence was recorded immediately using a luminometer (Lumat LB 9507; Berthold, Bad Wildbad, Germany).

The amount of firefly luciferase activity was normalized with reference to the protein concentration in the lysate. The protein was quantitated using the BCA Protein Assay Reagent kit (Pierce, IL), which is based on bicinchoninic acid.

Localization of sgRNA

The cytoplasmic fraction was prepared from collected cells after washing twice with phosphate-buffered saline (PBS). The cells were resuspended in digitonin lysis buffer (50 mM HEPES-KOH, pH 7.5, 50 mM potassium acetate, 8 mM $MgCl_2$, 2 mM EGTA and 50 μg/ml digitonin) and incubated on ice for 10 min. The lysate was centrifuged at 1000 *g* for 5 min and the resultant supernatant was collected and used as the cytoplasmic fraction. The pellets were resuspended in NP-40 lysis buffer (20 mM Tris–HCl, pH 7.5, 50 mM KCl, 10 mM NaCl, 1 mM EDTA and 0.5% NP-40) and incubated on ice for 10 min. The resultant lysate was used as the nuclear fraction. Cytoplasmic and nuclear RNA were extracted and purified

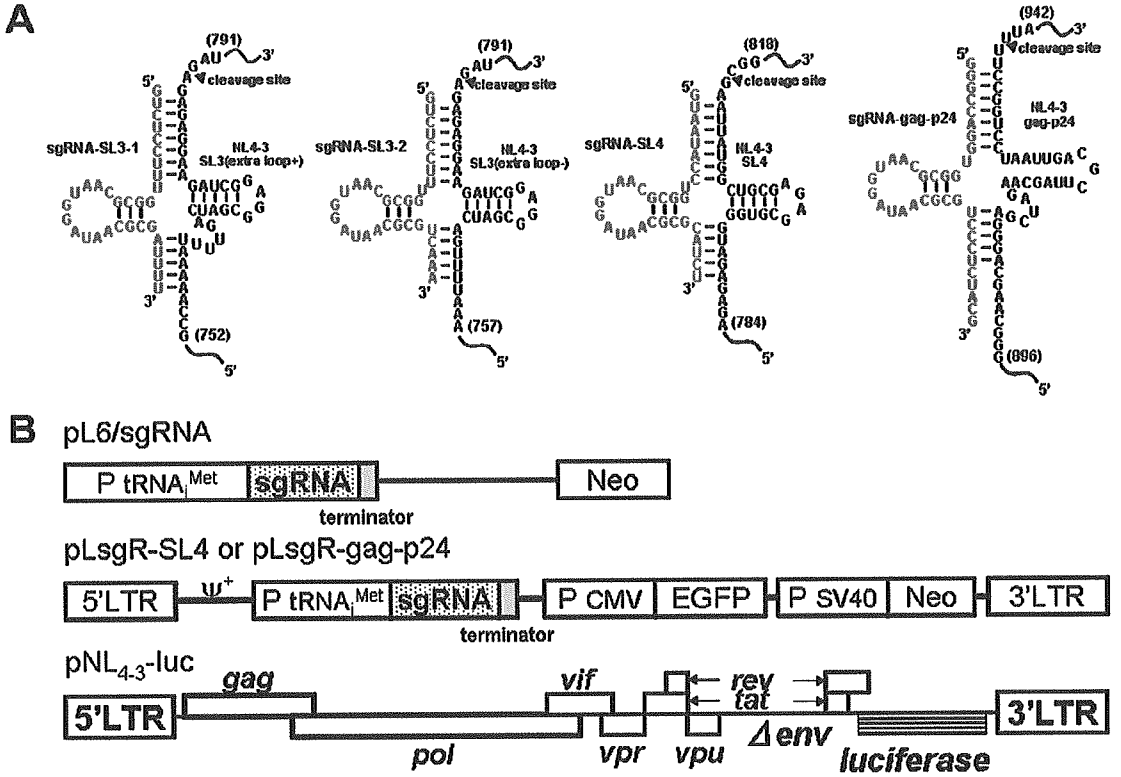

Figure 1. (A) Plausible secondary structures of complexes of the three target sites within the HIV-1 genome [the ψ site (SL3-stem loop), the SL4-stem-loop site and gag-24 within the HIV-1 gene] with the modified 5′-half-tRNA^{Arg} (sgRNA-SL3-1, 2, SL-4 and gag-p24) containing 7 and 5 nt sequences complementary to the target HIV-1 ψ site and the *gag* gene. The arrow indicates the tRNase Z cleavage point. (B) Schematic diagrams of the sgRNA-expression plasmids, the retroviral vector and the HIV-1 luciferase reporter-vector constructs. Methods for the construction of the sgRNA-expression plasmids (pL6-sgRNA-SL3-1, pL6-sgRNA-SL3-2, pL6-sgRNA-SL4 and pL6-sgRNA-gag-p24) and the retroviral vectors (pLsgRGSN-SL4 and pLsgRGSN-gag-p24) are detailed in Materials and Methods. The envelope-defective HIV-1 NL_{4-3}-based retroviral vector contained a luciferase-expression marker (pNL_{4-3}-luc). This HIV-1-based vector was generated by substituting the *nef* gene sequences of the HIV-1_{NL4-3} genome with the firefly luciferase gene, and deleting the envelope gene sequences located between two Bgl II restriction endonuclease sites (32).

from their respective fractions using ISOGEN reagent (Wako, Osaka, Japan). RNA samples were treated with DNase I (Takara Shuzo, Shiga, Japan) according to the manufacturer's instructions. RT–PCR assays were performed using an RT–PCR High-Plus kit (Toyobo, Osaka, Japan) according to the manufacturer's protocol. The nucleotide sequences of the sgRNA-SL4 primers were 5′-TACTGTGAGACCGTGTGCTT-3′ (F-primer) and 5′-TACTGTGAGACCGTGTGCTT-3′ (R-primer). The nucleotide sequences of the U6 primers were 5′-CAGACATGATAAGATACATTGATGAGTTTG-3′ (F-primer) and 5′-CGGGATCCCGGCAATAGCATCACAAATTTC-3′ (R-primer).

Cleavage activities of sgRNA in COS cells

COS cells were grown to ~80% confluence (3×10^5 cells) and transfected with 3 μg each of the sgRNA vector and the pNL_{4-3}-luc plasmid. The cells were incubated for 2 days before total cellular RNA was isolated. RNA samples were treated with DNase I according to the manufacturer's specifications, and RT–PCR assays were carried out as described above. The levels of cleaved and uncleaved HIV-1 mRNAs were quantified by RT–PCR with an endogenous internal standard, GAPDH. A sample of 1 μg of total RNA was used as the template with the SL3, SL4, p24 and GAPDH primers (20 pmol each). Reverse transcription in a final reaction volume of 50 μl was carried out at 60°C for 30 min. The cDNA products were then amplified by PCR using amplification conditions comprising 40 cycles of 94°C for 60 s and 60°C for 90 s. The SL3-F1 (5′-TTGCTGAAGCGCGCACGGCA-3′) and p24-F1 (5′-TAAGGCCAGGGGGAAAGAAACAATATAAAC-3′) primer pair, and the SL3-R and SL4-R (5′-GTTCTTCTGATCCTGTCTGAAGGGATGGTT-3′) and p24-R (5′-GCCCCTGGAGGTTCTGCACTATAGGGTAAT-3′) primer pair, only generated a cDNA product from the uncleaved HIV-1 mRNA (RT–PCR products I and III, SL3 = 310 bp; RT–PCR product V, gag-p24 = 360 bp). The SL3-F2 (5′-TAAATGGGAAAAAATTCGGT-3′), SL4-F2 (5′-ATTCGGTTAAGGCCAGGGGG-3′) and p24-F2 (5′-AGACAAATACTGGGACAGCTACAACCATCC-3′) primer pairs were used to generate cDNA products corresponding to the cleaved and uncleaved sgRNA sequences, respectively, thereby identifying both sets of products. The SL3, SL4 and p24 yielded the RT–PCR products II (SL3 = 182 bp), IV (SL4 = 168 bp) and VI (p24 = 250 bp), whereas the GAPDH-F and R-primers amplified a fragment of the GAPDH gene (0.45 kb) as an internal control.

In vitro RNA synthesis

The partial HIV-1 RNA targets (T-SL3-1 and T-gag-p24) and the sgRNAs (sgRNA-SL3-1 and sgRNA-gag-p24) were synthesized from the corresponding synthetic DNA templates with an additional unencoded 'G' at the 5′ end corresponding to the −1 in a tRNA to enhance its transcriptional efficiency, using T7 RNA polymerase (Takara Shuzo). The sequences of the target RNAs and sgRNAs were as follows: 5′-GCCAAAAAUUUUGACUAGCGGAGGCUAGAAGGAGAGAGAUGGGUGC-3′ (T-SL3-1); 5′-GCAAGCAGGGAGCUAGAACGAUUCGCAGUUAAUCCUGGCCUUUUAGAGACA-3′ (T-gag-p24); 5′-GUCUCCUUUGGCGCAAUGGAUAACGCGAUUUU-3′ (sgRNA-SL3-1); and 5′-GGGCCAGGUGGCGCAAUGGAUAACGCGUCCCUCUACG-3′ (sgRNA-gag-p24). The transcription reactions were carried out under the conditions recommended by the manufacturer (Takara Shuzo), and after synthesis the RNAs were purified by denaturing gel electrophoresis. The RNA transcripts for T-SL3-1 and T-gag-p24 were subsequently labelled with fluorescein (F) according to the manufacturer's protocol (Amersham Pharmacia Biotech, NJ). Briefly, after the removal of the 5′-phosphates of the transcribed RNAs using bacterial alkaline phosphatase (Takara Shuzo), the RNAs were phosphorylated with T4 polynucleotide kinase (Takara Shuzo) and ATPγS. Then, a single fluorescein moiety was appended to the 5′-phosphorothioate site. The resulting fluorescein-labelled RNAs were gel-purified before being used in the assays.

In vitro RNA-cleavage assays

The *in vitro* RNA-cleavage assays for the fluorescein-labelled target RNA, T-SL3-1 or T-gag-p24 (0.1 pmol), were performed with pig liver tRNase ZL (20 ng) in the presence of unlabelled sgRNA-SL3-1 or sgRNA-gag-p24 (5 or 10 pmol) in a mixture (6 µl) containing 10 mM Tris–HCl (pH 7.5), 1.5 mM DTT and 10 mM $MgCl_2$ at 50°C for 10 min. After resolution of the reaction products by electrophoresis through a 10% polyacrylamide/8 M urea sequencing gel, the gel was analysed using a Typhoon 9210 (Amersham Pharmacia Biotech).

HIV-1-challenge assay

G418-resitant cell pools were incubated for 4 h with HIV-1_{NL4-3} at a multiplicity of infection of 0.01. After two washes with PBS, the cells were cultured in RPMI 1640 medium (Sigma) supplemented with 10% (v/v) heat-inactivated FBS. The supernatant was collected on days 1, 3, 6, 9, 12, 15 and 18 after viral infection, and the culture medium was assayed for HIV-1 gag-p24 antigen using CLEIA (Lumipulse, Fujirebio, Tokyo, Japan) according to the manufacturer's protocol (37).

RESULTS AND DISCUSSION

sgRNAs can inhibit HIV-1 gene expression

We demonstrated in a previous study that antisense phosphorothioate oligonucleotides (S-ODNs) complementary to the *gag* mRNA (SL4-stem loop), containing the HIV-1 *gag* AUG initiation codon, have potent anti-HIV activity in infected cultured cells. This activity was strong compared with oligonucleotides targeted to the splice acceptor of the *tat* gene and the AUG initiation codon of the *rev* gene (38). We have also shown *in vitro* that mammalian tRNase ZL with the aid of a 5′-half-tRNA-like sgRNA can cleave a partial HIV-1 mRNA substrate containing the p24 site of the HIV-1 *gag* gene (24). Therefore, it would be reasonable to select the gag AUG site (designated SL4) and the gag-p24 site to examine the efficacy of the sgRNA method in cultured cells. The HIV-1 packaging signal (ψ) that efficiently targets genomic RNA into nascent virions (39,40) and the ψ site (designated SL3) was chosen as an additional target site for tRNase ZL.

The 5′-half-tRNA-type sgRNAs, designated sgRNA-SL3-1 and sgRNA-SL3-2 (extra loop-), were designed to form

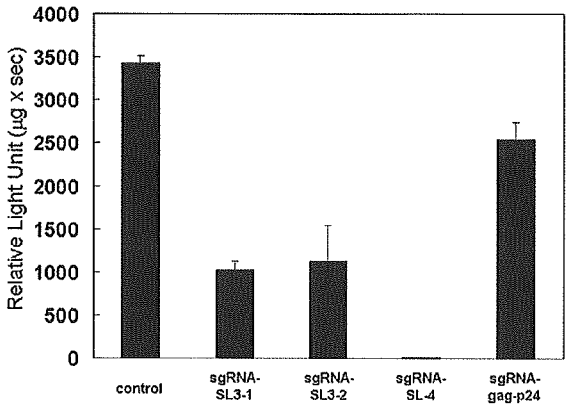

Figure 2. Luciferase activity of the pNL_{4-3}-luciferase (pNL_{4-3}-luc) fusion gene in COS cells. The cells were co-transfected with the target-expressing plasmid pNL_{4-3}-luc and either the pL6 plasmid encoding the sgRNAs or pL6-ter serving as a negative control for inhibition using the FuGENE™6 transfection reagent. The plotted data were averaged from three independent experiments, and the bars represent ±SD.

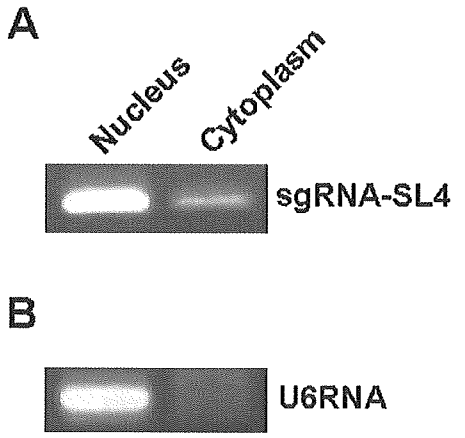

Figure 3. Intracellular localization of the $tRNA_i^{met}$–sgRNA. To analyse the degree of intracellular localization of $tRNA_i^{met}$–sgRNA, nuclear and cytoplasmic fractions were prepared from transformants that expressed sgRNA-SL4 and the total RNA was extracted from each. The transcribed sgRNA-SL4 was detected using RT–PCR analysis with a primer specific for the sgRNA. (**A**) RT–PCR analyses revealed that $tRNA_i^{met}$–sgRNA-SL4 was located almost exclusively in the nucleus, as predicted. (**B**) Nuclear and cytoplasmic fractions were examined with a probe specific for the transcript of the U6 gene (control).

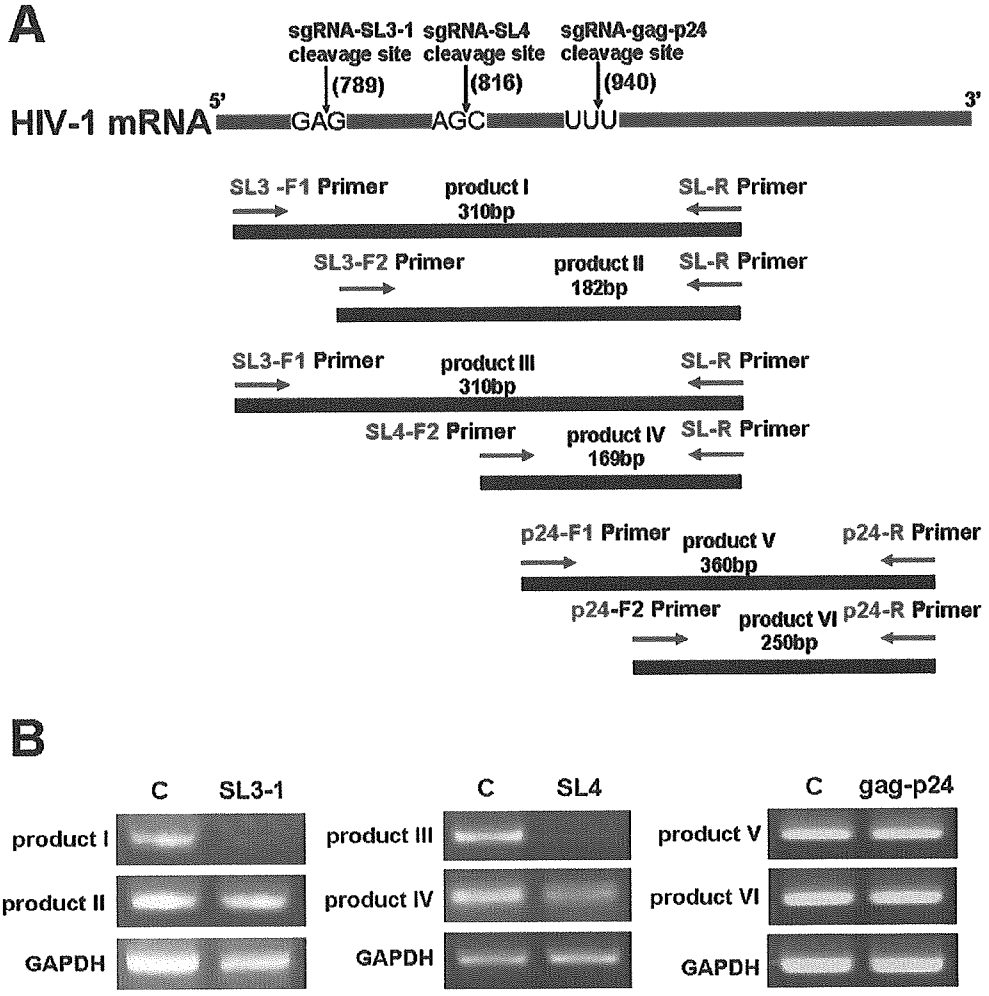

Figure 4. RT–PCR analyses of HIV-1 mRNA expression. RT–PCR analyses of uncleaved (product I), and total cleaved and uncleaved (product II), HIV-1 mRNA were performed using HIV-1 *gag*-specific primers with concurrent amplification of GAPDH mRNA. (**A**) Schematic representation of HIV-1-specific primer sites with respect to HIV-1 mRNA: F1 primers, SL3 and p24; F2 primers, SL3, SL4 and p24; R-primers, SL3, SL4 and p24. (**B**) RT–PCR amplification products analysed by 2% agarose gel electrophoresis with ethidium bromide staining.

pre-tRNA-like complexes with SL3. They contained or lacked an extra loop, respectively (Figure 1A). sgRNA-SL4 without an extra loop was intended to make a pre-tRNA-like complex with SL4, and sgRNA-gag-p24 with an extra loop was designed to form a pre-tRNA-like complex with the gag-p24 site (Figure 1A).

The sgRNA-expression plasmids were constructed in the mammalian expression plasmid pL6 (41,42) and (Figure 1B) by inserting synthetic DNA sequences between the human $tRNA_i^{met}$ promoter sequence and the RNA polymerase III termination-signal sequence. RT–PCR analysis was used to examine the expression of the sgRNA by these plasmids in transfected COS cells. A high level of sgRNA was expressed in the transfected cells, driven by a $tRNA_i^{met}$ promoter (data not shown).

A transient-expression assay was used to test the ability of pL6-expressed sgRNA-SL3-1 and 2, sgRNA-SL4 and sgRNA-gag-p24 to inhibit HIV-1 expression. COS cells were co-transfected with the sgRNA plasmids and an HIV-1_{NL4-3}-based vector containing a luciferase-expression maker (pNL_{4-3}-luc) (31), then suppression of HIV-1 was assessed in a single-cycle infectivity assay (Figure 2). HIV-1_{NL4-3}-based luciferase activity was recorded using the control plasmid vector L6-ter with only the $tRNA_i^{met}$ promoter and terminator sequences, rather than the sgRNA-expression plasmid. Both sgRNA-SL3-1 and sgRNA-SL3-2 showed good inhibition of HIV-1 expression in the cultured cells, suggesting that the extra loop in the pre-tRNA-like complex is not important for tRNase ZL recognition (Figure 2). Amazingly, HIV-1 gene expression was almost completely inhibited by sgRNA-SL4, but only moderately suppressed by sgRNA-gag-p24. This might be because endogenous tRNase ZL has difficulty in recognizing the sgRNA-gag-p24/target complex, possibly due to the lack of a stable 'T-stem-loop' structure in the target, as indicated by the *in vitro* cleavage assays described below. These results imply that the sgRNA/tRNase

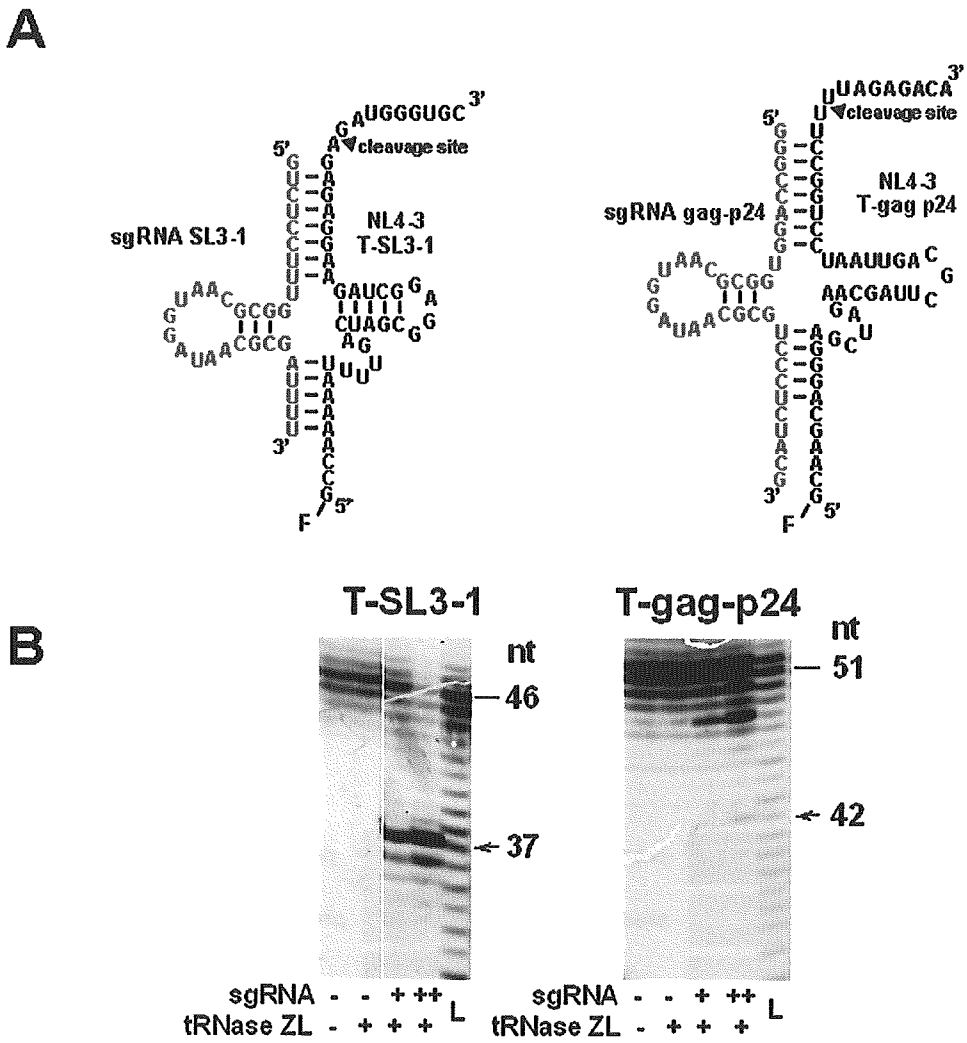

Figure 5. sgRNA guided specific HIV-1 mRNA cleavage by *in vitro* tRNase ZL assays. (**A**) Secondary structures of the substrate-HIV-1 SL3-1 (extra loop) and gag-24 complexes with sgRNA-SL3-1 and sgRNA-gag-p24. (**B**) The assays for the fluorescein (F)-labelled target RNA T-SL3-1 or T-gag-p24 (0.1 pmol) were performed with pig liver tRNase ZL (20 ng) in the presence of the unlabelled sgRNA-SL3-1 or sgRNA-gag-p24 (5 or 10 pmol) at 50°C for 10 min. The cleavage reactions were analysed using a 10% polyacrylamide/8 M urea sequencing gel. The target RNA and the primary 5′-cleavage product are indicated by a bar and arrow, respectively, together with their size in nucleotides. L denotes the alkaline ladder of each fluorescein-labelled target RNA.

ZL strategy is effective in reducing the level of the HIV-1 gene expression, although the efficiency of inhibition differs according to the sgRNAs used.

Intracellular localization of the $tRNA_i^{met}$–sgRNA

Co-localization of sgRNAs, their RNA targets and tRNase ZL is important for efficient downregulation; therefore, we examined the intracellular location of sgRNA-SL4 (41,42). Transformed cells expressing sgRNA-SL4 were separated into nuclear and cytoplasmic fractions, and the total RNA was extracted from each. sgRNA-SL4 was detected using RT–PCR analysis with a primer specific for the sgRNA. This revealed that they were located almost exclusively in the nucleus (80%) (Figure 3).

The inhibitory effect of sgRNA occurs through target RNA degradation by tRNase ZL

The contribution of HIV-1 mRNA cleavage to the sgRNA-mediated anti-HIV-1 effect was examined by measuring HIV-1 mRNA levels (43,44). Two sets of RT–PCR reactions were used to establish the level of HIV-1 mRNA uncleaved at the target site by tRNase ZL [products I (310 bp), III (310 bp) and V (360 bp)], and the total amount of HIV-1 mRNA at the target site [products II (182 bp), IV (169 bp) and VI (250 bp)], i.e. both cleaved and uncleaved. The uncleaved HIV-1 mRNA was amplified by primers SL3-F1 and gag-p24-F1, and the SL3-R, SL4-R and gag-p24-R primers (Figure 4A). The levels of products I, III and V were expected to decrease after cleavage of the HIV-1 mRNA. The levels of products II, IV and VI reflected the total amount of HIV-1 mRNA (cleaved and

uncleaved SL3, SL4 and gag-p24), as the 3′ fragment of cleaved HIV-1 mRNA remained a viable template for amplification in this PCR. The results, which are shown in Figure 4B, indicate that the sgRNA-SL3-1- and SL4-dependent expression system reduced the amount of HIV-1 mRNA [products I (92%) and IV (97%)], whereas transfection with pNL_{4-3}-luc/sgRNA-gag-p24 did not significantly alter uncleaved HIV-1 mRNA expression in COS cells (Figure 4B). These data are consistent with the results of the luciferase assays and suggest that the inhibitory effect of sgRNA is achieved through target RNA degradation by tRNase ZL.

sgRNA-gag-p24 barely directs *in vitro* HIV-1 RNA cleavage by tRNase ZL

sgRNA-gag-p24 was much less effective than the other sgRNAs in suppressing HIV-1 gene expression in cells. We examined the reason for this by assessing its ability to guide HIV-1 RNA cleavage by tRNase ZL *in vitro*. The partial HIV-1 RNAs T-SL3-1 and T-gag-p24 containing SL3 and the gag p24 site, respectively, were synthesized *in vitro* with T7 RNA polymerase and 5′ end-labelled with fluorescein. sgRNA-SL3-1 and sgRNA-gag-p24 were also transcribed by T7 RNA polymerase *in vitro*. The ability of each sgRNA to induce cleavage of the corresponding target RNA by tRNase ZL was tested *in vitro*. The target T-SL3-1 was cleaved efficiently under the direction of sgRNA-SL3-1, whereas cleavage of the target T-gag-p24 by sgRNA-gag-p24 was highly inefficient (Figure 5), this was in agreement with the *in vivo* observations. Cleavage of each target occurred primarily 1 nt downstream of the nucleotide corresponding to the discriminator (Figure 5). These results indicate that sgRNA bound to its target HIV-1 mRNA, and cleavage of the pre-tRNA complexes with tRNase ZL occurred. It was therefore important to determine the localization of both the sgRNA and its target HIV-1 in the cells. The reduction in functional HIV-1 mRNA was consistent with tRNase ZL cleavage occurring at the post-transcriptional level.

Inhibition of HIV-1 gene expression by retroviral vector-mediated sgRNAs in human T cells

The inhibitory effect of HIV-1 expression by tRNase ZL-mediated sgRNAs was investigated in human T cells by constructing a MoMLV-based sgRNA retroviral vector. Most retroviral vectors used in experimental and clinical gene therapy are derived from the MoMLV (45). Retroviruses integrate into the chromosomal DNA, so their genome is stable in the host cells and is inherited by their progeny. Accordingly, long-term expression of a transduced gene can be achieved through retrovirus-mediated gene transfer. Other advantages of this vector include its broad host range and the availability of packaging cell lines for the large-scale production of high-titre vectors. It has previously been shown that an amphotropic MoMLV-based retrovirus vector can transduce a human T-cell line (46). We therefore expressed the sgRNA under the control of the promoter of a human $tRNA_i^{met}$ gene via a retroviral vector (Figure 1B). The plasmid pLsgRGSN (Figure 1B) was constructed by inserting the following elements into the EcoRI and XhoI sites of the retroviral vector pLXSN: an EcoRI and XhoI fragment from the plasmid pSV2neo/sgRG, sgRNAs and EGFP genes. We then obtained transduced Jurkat T cells

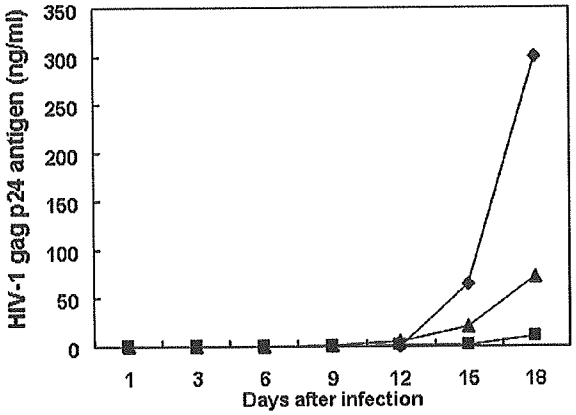

Figure 6. Inhibition of HIV-1 gag-p24 product in Jurkat cells expressing stably retrovirus vector-mediated sgRNA. Cells were cultured for 18 days after infection with $HIV\text{-}1_{NL4\text{-}3}$. Small aliquots of supernatant were prepared from each culture on days 1, 3, 6, 9, 12, 15 and 18. HIV-1 gag p24 antigen was determined using CLEIA (Lumipulse) according to the manufacturer's protocol (37): closed diamonds, pLGSN-Δ*sgR*; closed squares, pLsgRGSN-SL4; and closed triangles, pLsgRGSN-gag-p24.

stably expressing the sgRNAs. These Jurkat T cells were infected with wild-type $HIV\text{-}1_{NL4\text{-}3}$, and HIV-1gag-p24 antigen levels in the cell-free supernatant were measured at weekly intervals over 18 days. By day 18, the HIV-1 gag-p24 product was suppressed almost completely (~97%) in the cell cultures expressing sgRNA-SL4 (Figure 6). In contrast, sgRNA-gag-p24 and sgRNA-SL4 failed to inhibit viral expression under these experimental conditions. The difference between the effects of sgRNA-SL4 and sgRNA-gag-p24 in the HIV-1-challenged assay was due to the lack of base pairing in the hairpin structure resembling the T-stem-loop region.

In conclusion, we demonstrated the inhibition of HIV-1 gene products in cultured cells by inducing HIV-1 mRNA cleavage using a modified 5′-half-$tRNA^{Arg}$ (sgRNA) and mammalian tRNase ZL. The sgRNA/target HIV-1RNA complex formed a pre-tRNA-like structure with 5′-half-tRNA and a stable hairpin (3′-half-tRNA) structure resembling the T-stem-loop region. The $tRNA_i^{met}$–sgRNA transcript was expressed at high levels and localized in the nucleus. The greatest inhibitory effect on HIV-1 expression was achieved using sgRNA-SL4 targeting the HIV-1 *gag* gene. These results suggest that both sgRNA and its target HIV-1 mRNA were located in the nucleus, allowing specific cleavage by tRNase ZL. Furthermore, MoMLV-based sgRNA-SL4 could suppress sgRNA-dependent HIV-1 expression in human T cells. We believe that the use of mammalian tRNase ZL in conjunction with guide sequences represents a promising tool for the inactivation of genes in mammalian cells. Furthermore, the inhibition of HIV-1 using this approach demonstrates its potential as a therapeutic agent for AIDS.

ACKNOWLEDGEMENTS

We thank Prof. Y. Koyanagi for providing some of the plasmids, and Dr H. Takeuchi for technical assistance. This work was supported by a Grant-in-Aid for High Technology

Research (HTR) from the Ministry of Education, Science, Sports and Culture, Japan, by research grants from the Human Science Foundation (HIV-K-14719) and the Science Research Promotion Fund, and by an Academic Frontier Research Project Grant from the Promotion and Mutual Aid Corporation for the Private Schools of Japan. Y.H. is a Research Fellow of the HTR. Funding to pay the Open Access publication charges for this article was provided by HTR.

REFERENCES

1. Kelin,A.S., Klebba,C. and Hoelzer,D. (2000) Gene therapy of HIV-1 infection. In Unger,R.E., Kreuter,J. and Rubsaman-Waigmann,H. (eds.), *Antivirals Agent AIDS*. Marcel Dekker Inc., NY, 219–248.
2. Rigden,J.R., Ely,J.A., Macpherson,J.L., Gerlach,W.L., Sun,L.-Q. and Symonds,G.P. (1999) The use of ribozyme gene therapy for the inhibition of HIV replication and its pathogenic sequelae. In Rossi,J.J. and Couture,L.A. (eds.), *Intracellular Ribozyme Applications, Principles and Protocols*. Horizon Scientific Press, England, 93–102.
3. Dornburg,R. and Pomerantz,R.Z. (2000) Gene therapy and HIV-1 infection. In Templeton,N.S. and Lasic,D.D. (eds.), *Gene Therapy, Therapeutic Mechanisms and Strategies*. Marcel Dekker Inc., NY, 519–534.
4. Kurreck,J. (2003) Antisense technologies, improvement through novel chemical modifications. *Eur. J. Biochem.*, **270**, 1628–1644.
5. Jen,K.-Y and Gewirtz,A.M. (2000) Suppression gene expression by targeted disruption of messenger RNA available options and current strategies. *Stem Cells*, **18**, 307–319.
6. Bunnell,B.A. and Morgan,R.H. (1998) Gene therapy for infectious diseases. *Clin. Microbiol. Rev.*, **11**, 42–56.
7. Martinez,M.A., Clotet,B. and Este,J. (2002) RNA interference of HIV replication. *Trends Immunol.*, **23**, 559–561.
8. Lori,F., Guallini,P., Gulluzzi,L. and Lisziewicz,J. (2002) Gene therapy approaches to HIV infections. *Am. J. Pharmacogenomics*, **2**, 245–252.
9. Stevenson,M. (2003) Dissecting HIV-1 through RNA interference. *Nature Rev. Immunol.*, **3**, 851–858.
10. Scherer,L.J. and Rossi,J.J. (2003) Approaches for the sequence-specific knockdown of mRNA. *Nat. Biotechnol.*, **21**, 1457–1465.
11. Takaku,H. (2004) Gene silencing of HIV-1 by RNA interference. *Antivir. Chem. Chemother.*, **15**, 57–65.
12. Yuan,Y., Hwang,E.S. and Altman,S. (1992) Targeted cleavage of mRNA by human RNase P. *Proc. Natl Acad. Sci. USA*, **89**, 8006–8010.
13. Yuan,Y. and Altman,S. (1994) Selection of guide sequences that direct efficient cleavage of mRNA by human ribonuclease. *Science*, **263**, 1269–1273.
14. Guerrier-Takada,C., Li,Y. and Altman,S. (1995) Artificial regulation of gene expression in *Escherichia coli* by RNase P. *Proc. Natl Acad. Sci. USA*, **92**, 11115–11119.
15. Hnatyszyn,H., Spruillm,G., Youngm,A., Seivrightm,R. and Kraus,G. (2001) Long-term RNase P-mediated inhibition of HIV-1 replication and pathogenesis. *Gene Ther.*, **24**, 1863–1871.
16. Kraus,G., Geffin,R., Spruill,G., Young,A.K., Seivright,R., Cardona,D., Burzawa,J. and Hnatyszyn,H.J. (2002) Cross-clade inhibition of HIV-1 replication and cytopathology by using RNase P-associated external guide sequences. *Proc. Natl Acad. Sci. USA*, **99**, 3406–3411.
17. Barnor,J.S., Endo,Y., Habu,Y., Miyano-Kurosaki,N., Kitano,M., Yamamoto,H. and Takaku,H. (2004) Effective inhibition of HIV-1 replication in cultured cells by external guide sequences and ribonuclease P. *Bioorg. Med. Chem. Lett.*, **14**, 4941–4944.
18. Nashimoto,M. (1997) Distribution of both lengths and 5′ terminal nucleotides of mammalian pre-tRNA 3′ trailers reflects properties of 3′ processing endoribonuclease. *Nucleic Acids Res.*, **25**, 1148–1154.
19. Takaku,H., Minagawa,A., Takagi,M. and Nashimoto,M. (2003) A candidate prostate cancer susceptibility gene encodes tRNA 3′ processing endoribonuclease. *Nucleic Acids Res.*, **31**, 2272–2278.
20. Takaku,H., Minagawa,A., Takagi,M. and Nashimoto,M. (2004) The N-terminal half domain of the long form of tRNase Z is required for the RNase 65 activity. *Nucleic Acids Res.*, **32**, 4429–4438.
21. Tavtigian,S.V., Simard,J., Teng,D.H., Abtin,V., Baumgard,M., Beck,A., Camp,N.J., Carillo,A.R., Chen,Y., Dayananth,P. *et al.* (2001) A candidate prostate cancer susceptibility gene at chromosome 17p. *Nature Genet.*, **27**, 172–180.
22. Minagawa,A., Takaku,H., Takagi,M. and Nashimoto,M. (2004) The missense mutations in the candidate prostate cancer gene *ELAC2* do not alter enzymatic properties of its product. *Cancer Lett.*, in press.
23. Nashimoto,M. (1995) Conversion of mammalian tRNA 3′ processing endoribonuclease to four-base-recognizing RNA cutters. *Nucleic Acids Res.*, **23**, 3642–3647.
24. Nashimoto,M. (1996) Specific cleavage of target RNAs from HIV-1 with 5′ half tRNA by mammalian tRNA 3′ processing endoribonuclease. *RNA*, **2**, 523–534.
25. Nashimoto,M., Geary,S., Tamura,M. and Kaspar,R. (1998) RNA heptamers that direct RNA cleavage by mammalian tRNA 3′ processing endoribonuclease. *Nucleic Acids Res.*, **26**, 2565–2571.
26. Nashimoto,M. (2000) Anomalous RNA substrates for mammalian tRNA 3′ processing endoribonuclease. *FEBS Lett.*, **472**, 179–186.
27. Takaku,H., Minagawa,A., Takagi,M. and Nashimoto,M. (2004) A novel four-base-recognizing RNA cutter that can remove the single 3′ terminal nucleotides from RNA molecules. *Nucleic Acids Res.*, **32**, e91.
28. Tamura,M., Nashimoto,C., Miyake,N., Daikuhara,Y., Ochi,K. and Nashimoto,M. (2003) Intracellular mRNA cleavage by 3′ tRNase under the direction of 2′-*O*-methyl RNA heptamers. *Nucleic Acids Res.*, **31**, 4354–4360.
29. Cormack,B.P., Valdivia,R.H. and Falkow,S. (1996) FACS-optimized mutants of the green fluorescent protein (GFP). *Gene*, **173**, 33–38.
30. Yang,T.T., Cheng,L. and Kain,S.R. (1996) Optimized codon usage and chromophore mutations provide enhanced sensitivity with the green fluorescent protein. *Nucleic Acids Res.*, **24**, 4592–4593.
31. Miller,A.D. and Rosman,G.J. (1989) Improved retroviral vectors for gene transfer. *BioTechniques*, **7**, 980–987.
32. Akkina,R.K., Walton,R.M., Chen,M.L., Li,Q.-X., Planelles,V. and Chen,I.Y. (1996) High-efficiency gene transfer into CD34+ cells with a human immunodeficiency virus type 1-based retroviral vector pseudotyped with vesicular stomatitis virus envelope glycoprotein G. *J. Virol.*, **70**, 2581–2585.
33. Landau,N.R. and Littman,D.R. (1992) Packaging system for rapid production of murine leukemia virus vectors with variable tropism. *J. Virol.*, **66**, 5110–5113.
34. Li,X., Mukai,T., Young,D., Frankel,S., Law,P. and Wong-Staal,F. (1998) Transduction of $CD34^+$ cells by a vesicular stomach virus protein G (VSV-G) pseudotyped HIV-1 vector. Stable gene expression in progeny cells, including dendritic cells. *J. Hum. Virol.*, **1**, 346–352.
35. Burns,J.C., Friedmann,T., Driever,W., Burrascano,M. and Yee,J.-K. (1993) Vesicular stomatitis virus G glycoprotein pseudotyped retroviral vectors: concentration to very high titer and efficient gene transfer into mammalian and non-mammalian cells. *Proc. Natl Acad. Sci. USA*, **90**, 8033–8037.
36. Yee,J.K., Miyanohara,A., Laforte,P., Bouic,K., Burns,J.C. and Friedman,T. (1994) A general method for the generation of high-titer, pantropic retroviral vectors: highly efficient infection of primary hepatocytes. *Proc. Natl Acad. Sci. USA*, **91**, 9564–9568.
37. Sakai,A., Hirabayasi,Y., Aizawa,S., Tanaka,M., Ida,S. and Oka,S. (1999) Investigation of a new p24 antigen detection system by the chemiluminescence-enzyme-immunoassay. *J. Jap. Assoc. Infect. Dis.*, **73**, 205–212.
38. Kuwasaki,T., Hosono,K., Takai,K., Ushijima,K., Nakashima,H., Saito,T., Yamamoto,N. and Takaku,H. (1996) Hairpin antisense oligonucleotides containing 2′-methoxynucleosides with base-pairing in the stem region at the 3′-end: penetration, localization, and anti-HIV activity. *Biochem. Biophys. Res. Commun.*, **228**, 623–631.
39. Clever,J., Mirandar,D.Jr and Parslow,T.G. (2002) RNA structure and packaging signals in the 5′ leader region of the human immunodeficiency virus type 1 genome. *J. Virol.*, **76**, 12381–12387.
40. McBride,M.S. and Panganiban,A.T. (1997) Position dependence of functional hairpins important for human immunodeficiency virus type 1 RNA encapsidation *in vivo*. *J. Virol.*, **71**, 2050–2058.
41. Sullenger,B.A., Gallardo,H.F., Ungers,G.E. and Gilboa,E. (1990) Overexpression of TAR sequences renders cells resistant to human immunodeficiency virus replication. *Cell*, **63**, 601–608.
42. Sullenger,B.A., Lee,T.C., Smith,C.A., Ungers,G.E. and Gilboa,E. (1990) Expression of chimeric tRNA-driven antisense transcripts renders NIH 3T3 cells highly resistant to Moloney murine leukemia virus replication. *Mol. Cell. Biol.*, **10**, 6512–6523.

43. Zhang,Y.A., Nemunaitis,J., Scanlon,K.J. and Tong,A.W. (2000) Anti-tumorigenic effect of K-ras ribozyme against human lung cancer cell line heterotransplants in nude mice. *Gene Ther.*, **7**, 2041–2050.
44. Habu,Y., Miyano-Kurosaki,N., Nagawa,T., Matsumoto,N., Takeuchi,H. and Takaku,H. (2002) Inhibition of HIV-1 replication by an HIV-1 dependent ribozyme expression vector with the Cre/loxP (ON/OFF) system. *Antivir. Chem. Chemother.*, **13**, 273–281.
45. Mulligan,R.C. (1993) The science of gene therapy. *Science*, **260**, 926–932.
46. Miller,A.D. and Rosman,G.J. (1989) Improved retroviral vectors for gene transfer. *BioTechniques*, **7**, 980–987.

J. Biochem. **138**, 583–592 (2005)
doi:10.1093/jb/mvi158

Solution RNA Structures of the HIV-1 Dimerization Initiation Site in the Kissing-Loop and Extended-Duplex Dimers

Seiki Baba[1], Ken-ichi Takahashi[1,2], Satoko Noguchi[1], Hiroshi Takaku[1], Yoshio Koyanagi[3], Naoki Yamamoto[4] and Gota Kawai[1,*]

[1]Department of Life and Environmental Sciences, Chiba Institute of Technology, 2-17-1 Tsudanuma, Narashino, Chiba 275-0016; [2]Department of Bioscience, Faculty of Bioscience, Nagahama Institute of Bio-Science and Technology, 1266 Tamura-cho, Nagahama, Shiga 526-0829; [3]Institute for Virus Research, Kyoto University, Kyoto 606-8507; and [4]AIDS Research Center, The National Institute of Infectious Diseases, Toyama 1-23-1, Shinjuku-ku, Tokyo 162-8640

Received April 27, 2005; accepted August 13, 2005

Dimer formation of HIV-1 genomic RNA through its dimerization initiation site (DIS) is crucial to maintaining infectivity. Two types of dimers, the initially generated kissing-loop dimer and the subsequent product of the extended-duplex dimer, are formed in the stem-bulge-stem region with a loop including a self-complementary sequence. NMR chemical shift analysis of a 39mer RNA corresponding to DIS, DIS39, in the kissing-loop and extended-duplex dimers revealed that the three dimensional structures of the stem-bulge-stem region are extremely similar between the two types of dimers. Therefore, we designed two shorter RNA molecules, loop25 and bulge34, corresponding to the loop-stem region and the stem-bulge-stem region of DIS39, respectively. Based upon the chemical shift analysis, the conformation of the loop region of loop25 is identical to that of DIS39 for each of the two types of dimers. The conformation of bulge34 was also found to be the same as that of the corresponding region of DIS39. Thus, we determined the solution structures of loop25 in each of the two types of dimers as well as that of bulge34. Finally, the solution structures of DIS39 in the kissing-loop and extended-duplex dimers were determined by combining the parts of the structures. The solution structures of the two types of dimers were similar to each other in general with a difference found only in the A16 residue. The elucidation of the structures of DIS39 is important to understanding the molecular mechanism of the conformational dynamics of viral RNA molecules.

Key words: DIS, HIV-1, NMR, RNA, structure.

Abbreviations: DIS, dimerization initiation site; HIV-1, human immunodeficiency virus type 1.

Two molecules of viral genomic RNA are packaged in a dimeric state in the virion of human immunodeficiency virus type 1 (HIV-1), and this dimer formation is crucial to maintaining their infectivity (*1–4*). Accumulating evidence from both *in vivo* and *in vitro* experiments has shown that the specific sequence, the dimerization initiation site (DIS) located close to the 5′ terminus of the genomic RNA, is required for spontaneous dimerization of HIV-1 RNA. DIS can form a stem-loop structure with a self-complementary sequence in the loop and a bulge in the stem (*5, 6*). The dimerization of DIS forms the kissing-loop dimer as the first step; then, their intramolecular stems are converted into intermolecular stems, generating the extended-duplex dimer (*7, 8*). This two step dimerization process is called the kissing-loop mechanism. The kissing-loop dimer is converted into the extended-duplex dimer by incubation at 55°C (*9, 10*) or by incubation at physiological temperature with the HIV-1 nucleocapsid protein, NCp7, which includes two basic regions and two zinc-fingers (*11*). A number of experiments have been performed to gain an understanding of the role of the zinc-fingers as well as the basic regions (*12–16*). Our previous results show that, for the two step dimerization from the kissing-loop dimer to the extended-duplex dimer, the two basic regions surrounding the N-terminal zinc finger of NCp7 have RNA chaperone activity by themselves, and the zinc fingers increase the efficiency of the activity (*17, 18*).

A number of three dimensional structural analyses using NMR and X-ray methods have been performed to determine the conformation of each region of DIS, the loop region in the kissing-loop (*19, 20*) or extended-duplex dimers (*21–24*), as well as the bulge-out region (*25–27*). However, our previous studies suggested that the 39mer RNA sequence, DIS39, which covers the entire bulge and loop regions, is necessary and sufficient for the two step dimerization (*28, 29*). Thus, it is still relevant to determine the structures of the kissing-loop and extended-duplex dimers for DIS39 with the same sequence and conditions.

In the present study, we designed two shorter RNA molecules, loop25 and bulge34; loop25 includes the loop-stem region of DIS39, and bulge34 includes the stem-bulge-stem region (Fig. 1), respectively we then determined the solution structures of loop25 in each of the kissing-loop and extended-duplex dimers as well as bulge34. By combining the structure parts, the solution structures of DIS39 in the kissing-loop and extended-duplex dimers were able to be determined.

*To whom correspondence should be addressed. Tel/Fax: +81-47-478-0425, E-mail: gkawai@sea.it-chiba.ac.jp

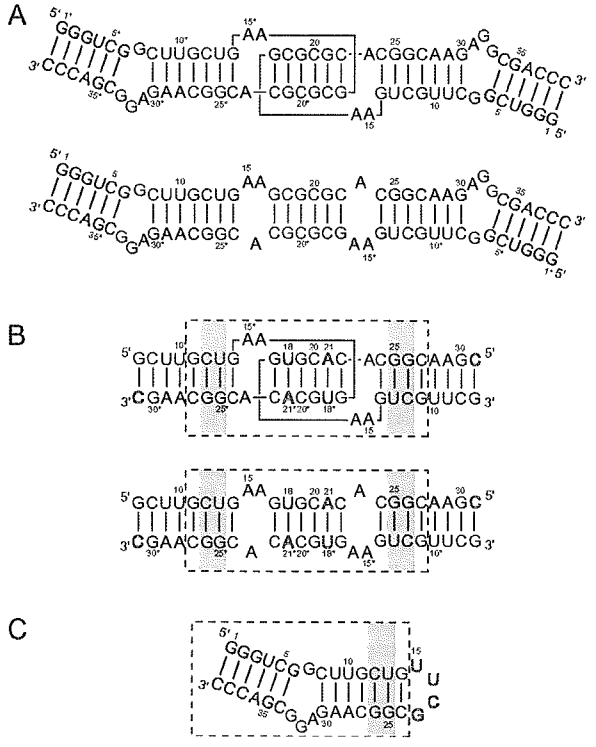

Fig. 1. **Secondary structure of a 39mer RNA corresponding to the dimerization initiation site (DIS39) and its fragments used in this study.** (A) The kissing-loop and extended-duplex dimers of DIS39. (B) The kissing-loop and extended-duplex dimers of loop25, which is composed of the loop and stem of DIS39. Modified residues are indicated by open characters. The sequence of the self-complementary loop was modified to increase the dispersion of NMR signals, and a base pair was added to the stem. The broken box indicates the part to be used for structure calculation. (C) Bulge34 consists of the stem-bulge-stem region of DIS39 and the connecting UUCG loop. The broken box indicates the part to be used for structure calculation. Gray shading indicates the two base pairs, C12–G26 and U13–G25, that are superimposed to combine the structures of the kissing-loop or extended-duplex dimer region and the stem-bulge-stem region. Asterisks indicate residues in the other strand.

MATERIALS AND METHODS

RNA Synthesis, Purification and Preparation—Nonlabeled loop25 was synthesized chemically by the phosphoramidite method with an automatic DNA/RNA synthesizer, Expedite model 8909 (PerSeptive Biosystems Inc., MA, USA). The protection groups were removed with ammonia and tetra-*n*-butylammonium fluoride. Nonlabeled DIS39 and bulge34 were synthesized enzymatically by the *in vitro* transcription reaction method with AmpliScribe T7 transcription kits (Epicentre Technologies Co., WI, USA). Purification for each RNA sample was performed by PAGE using 30 cm × 40 cm glass plates (Nihon Eido Co. Ltd., Tokyo, Japan) under denaturing conditions, and extensive desalting by ultrafiltration (Centricon YM3, Amicon Inc., MA, USA) was carried out. For stable isotopic labeling by the *in vitro* transcription with ^{13}C- and ^{15}N-labeled NTPs (Nippon Sanso, Tokyo, Japan), we used DIS39 rather than shorter loop25 and bulge34 because the efficiency of *in vitro* transcription is better for larger RNA.

For the preparation of the kissing-loop dimer, DIS39 or loop25 in water was incubated at 368 K for 5 min and chilled on ice for 5 min. Then, the solvent was adjusted to 1× PN-buffer [10 mM sodium phosphate (pH 7.0) and 50 mM NaCl] by adding concentrated buffer. For the preparation of the extended-duplex dimer, DIS39 or loop25 in 1× PN-buffer was incubated at 368 K for 5 min and slowly cooled to room temperature. Bulge34 was annealed by heating at 363 K for 5 min and snap-cooling on ice. To confirm the formation of the hairpin structure, the samples were subjected to a native PAGE experiment. For NMR measurements, RNA samples were dissolved in 10 mM sodium phosphate buffer (pH 7.0) containing 50 mM NaCl. The final concentration of chemically synthesized loop25 was 1.8 mM. The concentrations of DIS39 and bulge34 (transcripts) were 1.0 and 0.5 mM, respectively. The concentration of the kissing-loop and extended-duplex dimers of [G-$^{13}C/^{15}N$] and [A-$^{13}C/^{15}N$] DIS39 were 0.4, 0.3, 0.2 and 0.1 mM, respectively.

NMR Measurements—NMR spectra were recorded on Bruker DRX-500 and DRX-600 spectrometers. Spectra were recorded at probe temperatures of 283 to 303 K and NMR data at 298 K were used for structure calculation. The imino proton signal of the G and U residues in H_2O were distinguished from each other by the HSQC selected and HSQC filtered 1D spectra measured with ^{13}C and ^{15}N-labeled DIS39. Exchangeable proton NOEs were determined by 2D NOESY in H_2O with a mixing time of 150 ms using the jump-and-return scheme and gradient pulses for water suppression. For resonance assignments, well-established procedures were used (*30*). The H2 protons of adenosine were assigned based on a 2D HSQC experiment with natural abundance ^{13}C. NOE distance restraints from non-exchangeable protons were obtained from 2D NOESY experiments (mixing times of 50, 100, 200, and 400 ms) in D_2O. The intensities of the NOEs between exchangeable protons were interpreted as distances of 2.1–5.0 Å. For loop25, distances were estimated by analyzing the initial slope of NOE intensities for mixing times of 25, 50, 100, 200 ms. Judgment of intermolecular NOE is described in the result section. Two restraints (>5 Å) were added to the distance restraints based on the absence of NOE cross peaks in the case of the kissing-loop dimer. For bulge34, the intensities of NOEs due to nonexchangeable protons were interpreted as distances with a margin of −1.5 to +1.5 Å for the 100 ms 2D NOESY and −1.0 to +2.0 Å for the 200 ms 2D NOESY. Two restraints (>5 Å) were added to the distance restraints based on the absence of NOE cross peaks. The formation of hydrogen binding of G:C, A:U or G:U base pairs is interpreted as distance constraints as 1.8–2.1 Å for hydrogen and acceptor atoms and 2.8–3.2 Å for donor and acceptor atoms; G11:C27 to G14:C24, G11*:C27* to G14*:C24* and G17:C22* to C22:G17* for loop25 in the kissing-loop dimer, G11:C27* to G14:C24*, G11*:C27 to G14*:C24 and G17:C22* to C22:G17* for loop25 in the extended-duplex dimer, and G1:C39 to C5:G35 and U9:A29 to G14:C24 for bulge34. Dihedral restraints were obtained as described below. The absence of crosspeaks between H1′–H2′ in the 2D TOCSY and DQF-COSY experiments was interpreted as the residue being in the C3′-*endo*

conformation. On the other hand, the presence of strong crosspeaks between H1′–H2′ in the 2D TOCSY and DQF-COSY experiments was interpreted as the residue being in the C2′-*endo* conformation. The correction of sugar puckering is interpreted as dihedral restraints for ν_2 as 40.00 ± 20.00° (C3′-*endo*) or −35.00 ± 20.00° (C2′-*endo*). Based on the sequential connectivity of the Watson-Crick and G-U base pairs, the RNA-A conformation was assumed for the stem region and dihedral restraints were introduced for backbone torsion angles (α, β, γ, δ, ε and ζ) as the ideal conformation with a margin of ±10.00°. For loop25 in the kissing-loop dimer, information about the C3′-*endo* conformation (G11–G14, G17–C27), the C2′-*endo* conformation (A16) and RNA-A conformation in the stem region (G11–U13, U18–A21, G25–C27) was used as the dihedral restraints. For loop25 of the extended-duplex dimer, information about the C3′-*endo* conformation (G11–G14, G17-C27) and RNA-A conformation in the stem region (G11–U13, U18–A21, G25–C27) was used as the dihedral restraints. For bulge34, the information about the C3′-*endo* conformation (G1–G14, C24–A31, C34–C39) and RNA-A conformation in the stem region (G1–C5, G11–G14, C24–C27, G35–C39) was used as the dihedral restraints.

Structure Calculation—A set of 100 structures was calculated using the simulated annealing protocol described below with the InsightII/Discover package, and the amber force field was used. The force constants were 100 kcal mol^{-1} $Å^{-2}$ for distance restraints and 100 kcal mol^{-1} rad^{-2} for dihedral restraints. The starting coordinates were randomized, and the randomized structures were heated to 2,000 K in 5 ps, and the temperature was kept to 2,000 K for another 5 ps. After that, all restraints were increased to full values in 20 ps, then, decreased to 1/10 of full values in 5 ps at 2,000 K. Van der Waals radii were increased from 0.1 to 0.825 in 20 ps at 2,000 K. All restraints were increased to full value again in 10 ps at 2,000 K. Scalings for non-bond interactions were increased to full value in the next 20 ps at 2,000 K, and the temperature was kept to 2,000 K for another 5 ps. Then, the temperature was gradually scaled to 300 K in 10 ps. After that, the structure was heated from 300 to 1,000 K in 5 ps, and the van der Waals radii were increased from 0.825 to 1 at 1,000 K, and then decreased from 1 to 0.825 at 1,000 K. An additional 5 ps of dynamics was performed at 1,000 K, and the temperature was gradually scaled to 300 K for 10 ps. A final minimization step was performed, which included a Lennard-Jones potential and electrostatic terms with a dielectric constant of 7. The ten final structures with the lowest total energies were chosen.

RESULTS AND DISCUSSION

Analysis of the NMR Spectra of DIS39, Loop25 and Bulge34—Our previous NMR study revealed that the two types of dimers of DIS39 prepared as described in "MATERIALS AND METHODS" correspond to the kissing-loop and extended-duplex dimers (*31*). NMR spectra of DIS39 in each of the kissing-loop and extended-duplex dimers were measured in D_2O, and the signals due to H1′, H6/H8 were assigned by the sequential assignment method (Fig. 2). Figure 3A shows the difference in the chemical shift of H1′, H6/H8 between the two types of dimers. It was found that the difference is concentrated in the loop region. Interestingly, structures of the stem-bulge-stem region of the kissing-loop and extended-duplex dimers were extremely similar, even though the stems are formed by intra and inter molecules. This was also shown by analysis of the TOCSY spectrum; differences are located in the loop regions. Most residues were adapted to the C3′-*endo* conformation except for G32, G33 in the bulge-out region of both forms, A16 in the kissing-loop dimer and A15, A16 in the extended-duplex dimer, which might be a mixture of the C2′-*endo* and C3′-*endo* conformations.

To reveal further authentic structure, two RNA molecules were designed; loop25 includes the loop region and bulge34 includes the stem-bulge-stem region (Fig. 1, B and C). Loop25 was constructed to determine the authentic structure of the loop region. In order to increase the dispersion of the NMR signals, the sequence of the loop was modified from GCGCGC to GUGCAC. One base pair was added by replacing A31 by C31 in the stem to increase the stability of the kissing-loop dimer. It is noted that the loop sequences of GCGCGC and GUGCAC correspond to those of HIV-1 subtypes B and F (*32*), respectively, and both sequences have dimerization activity (*6, 9, 10*). The chemical shifts of loop25 were compared with those of DIS39 in each of the kissing-loop and extended-duplex dimers (Fig. 3, B and C). For both conformations, the chemical shifts for most of the stem region and A15, A16 and A23 were strikingly similar between the loop25 and DIS39. Due to the base alterations, the chemical shifts of the self complement loop were slightly different for both dimers. The chemical shift of H8 was shifted more than 0.2 ppm due to the addition of the terminal base pair. It is noteworthy that the chemical shift difference in loop25 between the kissing-loop and extended-duplex dimers (Fig. 3D) was almost identical to that of DIS39 (Fig. 3A). These results indicate that the structures of loop25 in the kissing-loop and extended-duplex dimers are essentially identical to those of DIS39. Upon analysis of the TOCSY spectrum, it was found that most of the residues were adapted to the C3′-*endo* conformation except A15 and A16 for the extended duplex dimer and A16 for the kissing loop dimer, and these results also agree with the results for DIS39.

Bulge34 was constructed to determine the authentic structure of the stem-bulge-stem region. Bulge34 consists of the stem-bulge-stem region of DIS39 and the connecting UUCG loop. The NMR signals of bulge34 were assigned by the sequential assignment technique. The chemical shift of H1′, H6/H8 of bulge34 were compared to those of DIS39 in the kissing-loop dimer (Fig. 3E). The chemical shifts for the stem-bulge-stem regions of bulge34 and DIS39 were identical, although the chemical shifts of the residues adjacent to the loop were slightly different by reflecting the difference in the closing loop sequences. Upon analysis of the TOCSY spectrum, it was found that most residues were adapted to the C3′-*endo* conformation except for G32, G33 in the bulge-out region and C in the UUCG loop, and that the conformation in the stem-bulge-stem region also agreed with that of DIS39. These results indicate that the structure of the stem-bulge-stem region of bulge34 is identical to that of DIS39.

Thus, the structures of DIS39 for two types of dimers can be determined by determining the structures of loop25 and bulge34, and combining them.

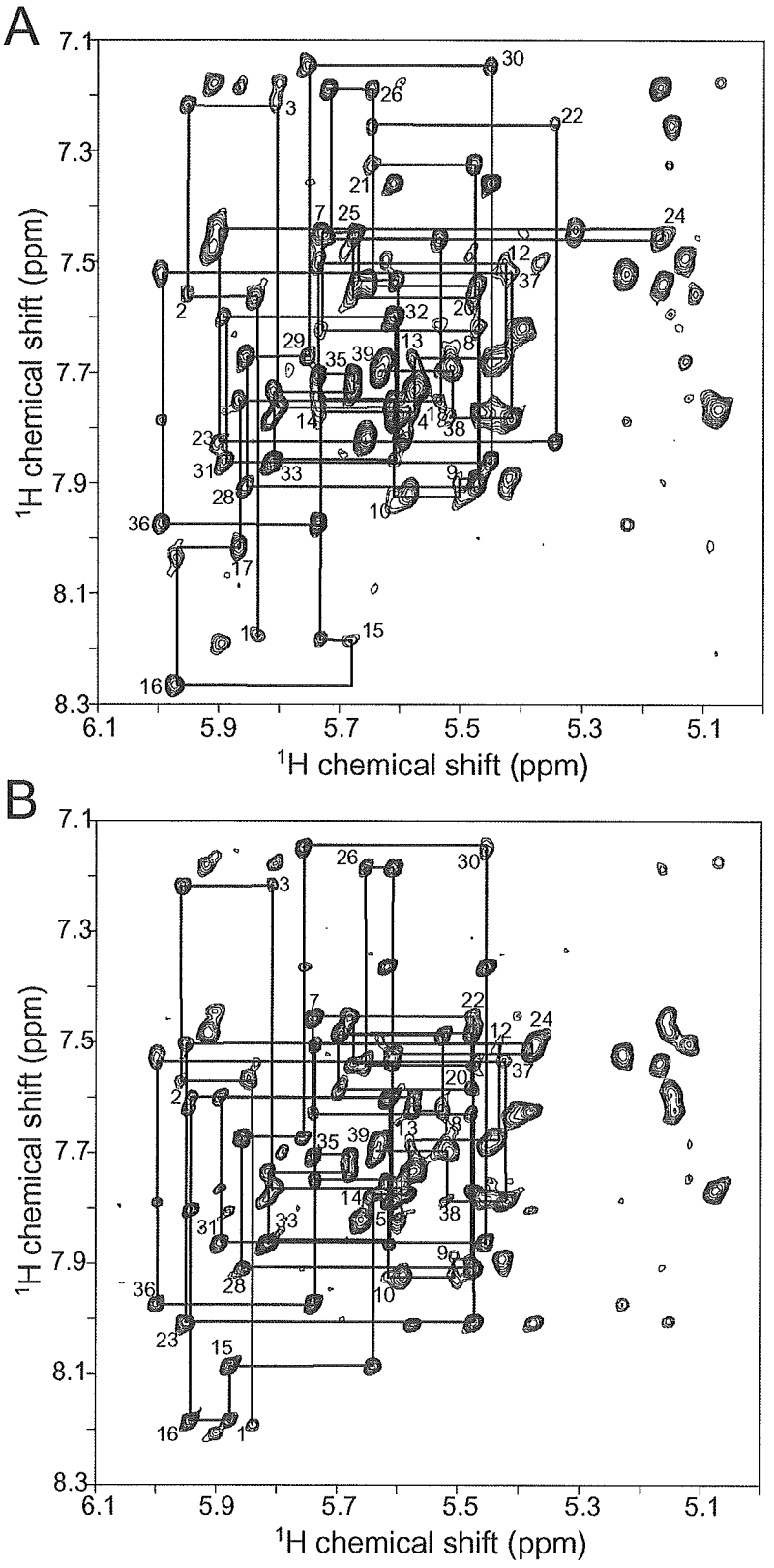

Fig. 2. **2D NOESY spectra of the (A) kissing-loop and (B) extended-duplex dimers of DIS39 measured in D_2O at 25°C with a mixing time of 200 ms.** Cross-peaks between aromatic H6/H8 protons and ribose H1′ protons are shown, and the sequential NOE connectivity is indicated.

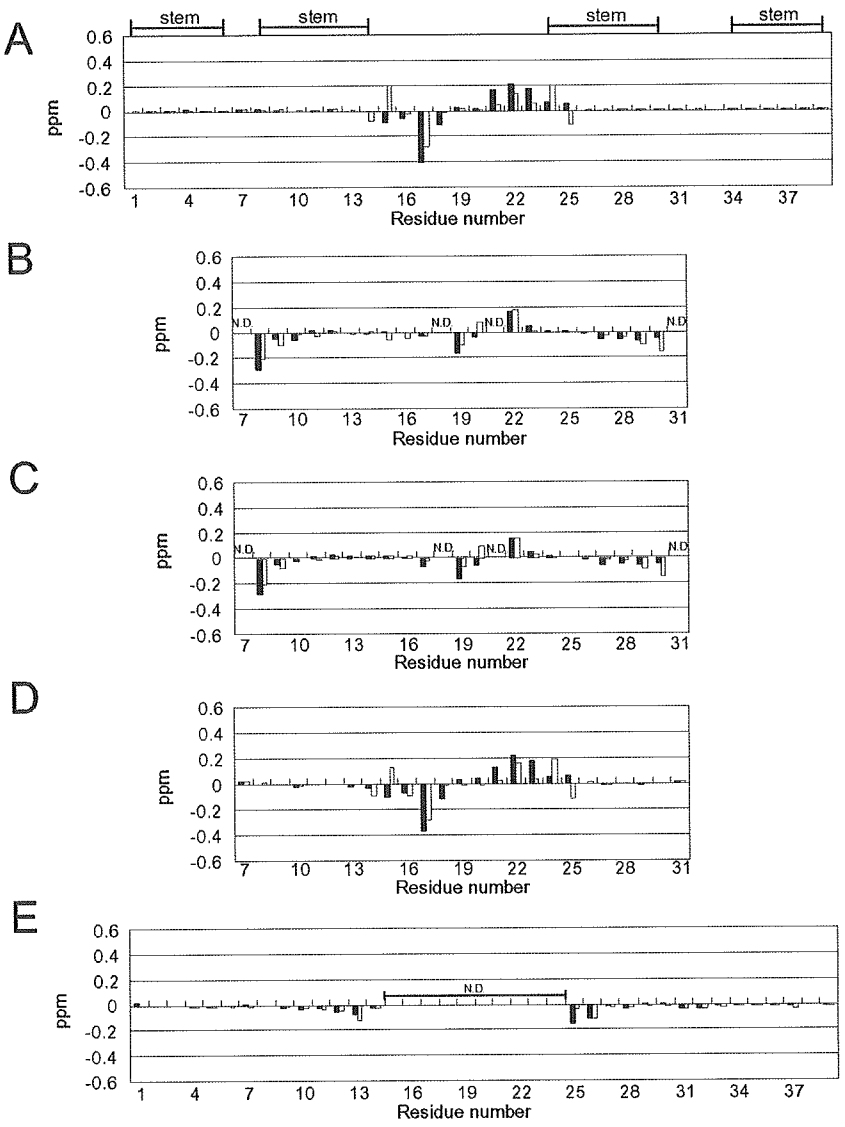

Fig. 3. **Chemical shift differences for H6/H8 and H1′.** Filled and open bars indicate H6/H8 and H1′, respectively. (A) Chemical shift differences between the kissing-loop and extended-duplex dimers of DIS39. Lines above the graph indicate the stem regions. (B) Chemical shift differences between DIS39 and loop25 in the kissing-loop dimer (data for replaced residues 7, 18, 21 and 31 are not shown). (C) Chemical shift differences between DIS39 and loop25 in the extended-duplex dimer (data for replaced residues 7, 18, 21 and 31 are not shown). (D) Chemical shift differences between the kissing-loop and extended-duplex dimers of loop25. (E) Chemical shift differences between DIS39 and bulge34 in the kissing-loop dimer (data for residues 15–24 are not shown).

Structure Determination—The loop region of loop25 in the kissing-loop dimer: To determine the structure of the loop region of DIS39 in both the kissing-loop and extended-duplex dimers, the NMR signals of loop25 were further analyzed and structural information was collected. The structure of the loop region consisting of the nine nucleotide loop and the stem with four base pairs was determined as shown by the broken box in Fig. 1B. A total of 286 distance restraints, 76 hydrogen bonding distance restraints, 140 dihedral restraints (Table 1), and 136 chiral restraints were used for the structural calculation. Three NOEs in the loop region, H2(A21)–H1′(U18), H2(A21)–H1′(G19) and H2(A21)–H8(G19), were judged to be intermolecular by analysis of the imino proton spectra. Four NOEs in the stem-loop linking region were considered to be intermolecular or intramolecular based on the results of the isotope filter NMR measurement (data not shown), and it was concluded that two NOEs, H2(A23)–H1′ (G17), H2(A16)–H1′ (G16), are intermolecular and three NOE, H8(A16)–H1′ (A16), H8(A16)–H2′ (A16), are intramolecular. One NOE in the stem-loop linking region was considered to be intermolecular or intramolecular in the structure calculation, and it was concluded that this NOE, H2(A23)–H2(A15), is intramolecular. Each restraint is used twice for two molecules. The structures were calculated by the restrained molecular dynamic calculation with the simulated annealing method. The structure was defined with a heavy atom r.m.s.d. of 2.14 Å for the ten converged structures (Fig. 4A, left panel), and the minimized average structure is shown in Fig. 4A (right panel). Although the overall convergence was not very good, the self-complementary region was well defined with 0.76 Å, and the stem-loop linking region was defined with 1.86 Å. The structural statistics are summarized in Table 1.

The loop region of loop25 in the extended-duplex dimer: The loop region of loop25 in the extended-duplex dimer was

Table 1. **NMR restraints and structural statistics.**

	Number of restraints		
	loop25 in the kissing-loop dimer (17 mer × 2)	loop25 in the extended-duplex dimer (17 mer × 2)	bulge34 (30 mer)
Distance restraints	286	384	345
imino-imino	12	12	10
intra residue	154	182	163
intra molecule	106	174	170
inter molecule	12	16	–
>5 Å	2	0	2
Hydrogen bonding distance restraints	76	76	58
Dihedral restraints	140	138	126
3′-*endo*	30	30	28
2′-*endo*	2	0	0
RNA-A stems	108	108	98
r.m.s.d. from the idealized geometry (Å)			
Bonds (Å)	0.00897 ± 0.00004	0.00803 ± 0.00020	0.00775 ± 0.00015
Angle (°)	2.43 ± 0.23	2.33 ± 0.05	2.24 ± 0.07
Impropers (°)	1.57 ± 0.10	1.82 ± 0.64	1.53 ± 0.21
Heavy-atoms r.m.s.d. (Å)[a]			
All	2.14	1.45	1.98
Stem-loop linking region[b]	1.86	1.31	
Bulge region[c]			1.90

[a]Averaged r.m.s.d. between an average structure and the 10 converged structures were calculated. The converged structures did not contain experimental distance violations >0.2 Å or dihedral violations >5°, [b]The stem-loop linking region consists of residues 14 to 17, 22 to 24, 14* to 17* and 22* to 24*, [c]The bulge region consists of residues 6 to 10 and 28 to 34. Asterisks indicate residues in the other molecule.

determined (broken box in Fig. 1B). A total of 384 distance restraints, 76 hydrogen bonding distance restraints, 138 dihedral restraints (Table 1) and 136 chiral restraints were used for the structure calculation. For the stem-loop linking region, H2 of A23 was connected by intermolecular NOEs to H1′ and H2 of A15, H2 of A16 and H1′ of G17. The structures were calculated by the restrained molecular dynamic calculation with the simulated annealing method described above. The structure was well defined with a heavy atom r.m.s.d. of 1.45 for the ten converged structures (Fig. 4B, left panel), and the minimized average structure is shown in Fig. 4B (right panel). The stem-loop linking region was defined with 1.31 Å. The structural statistics are summarized in Table 1.

The stem-bulge-stem region of bulge34: A structural determination was performed for bulge34 except for the UUCG loop (broken box in Fig. 1C). A total of 345 distance restraints, 58 hydrogen bonding distance restraints, 126 dihedral restraints (Table 1) and 120 chiral restraints were used for the structure calculation. Two NOE restraints (>5 Å), H2(A31)–H1′(U9) and H1′(A31)–H1′(U9), were added to the distance restraints based on the absence of NOE cross peaks. The structures were calculated by the restrained molecular dynamic calculation with a simulated annealing protocol. The structure was defined with a heavy atom r.m.s.d. of 1.98 for the ten converged structures (Fig. 4C, left panel), and the minimized average structure is shown in Fig. 4C (right panel). Although the overall convergence is not very good, the stem regions are well defined with 0.83 or 0.78 Å, respectively. The bulge region was defined with 1.90 Å. The structural statistics are summarized in Table 1.

The two types of dimers of DIS39: Solution structures of DIS39 were then constructed by combining the structure parts. The structures of the kissing-loop or extended-duplex dimer region and stem-bulge-stem region were combined by superimposing two base pairs, C12:G26 and U13:G25 (Fig. 1, gray area). The left panels of Fig. 5 show the ten structures prepared by using the minimized average structure of the stem-bulge-stem region (Fig. 4C, right) and each of the ten lowest energy structures of the loop region (Fig. 4, A or B, left) superimposed by the loop region. The right panels of Fig. 5 show the structures prepared using the minimized average structure of the stem-bulge-stem region (Fig. 4C, right) and the loop region (Fig. 4, A or B, right). The relative angles between the stem-bulge-stem regions differ between the kissing-loop and extended-duplex dimers as shown in the right panels of Fig. 5. However, the fluctuations of the relative angles are rather large and the ranges overlap between the two dimers as shown in the left panels of Fig. 5. In fact, the values of the residual dipolar coupling for the stem-bulge-stem region are similar between the kissing-loop and extended-duplex dimers (to be published). A preliminary normal mode analysis suggested the existence of hinge motion, and, in order to reveal the dynamic properties of the dimers, a molecular dynamics analysis, as well as the thermodynamics analysis (*33*), is required. The most obvious local difference was observed for A16; for the kissing-loop dimer, A16 was close to the same residue in the other molecule (Fig. 6A, left) and did not stack above A15 of the same molecule nor G17 of the other molecule (Fig. 6A, right), whereas for the extended-duplex dimer, A16 was apart from the same residue of the other molecule (Fig. 6B, left) and stacked between A15 and G17 (Fig. 6B, right).

Structural Comparison with Related Structures—Ennifar *et al.* (*20*) determined the crystal structure of